Nigerian Journal of Technology (NIJOTECH)
Vol. 41, No. 1, January, 2022, pp.148 –157
www.nijotech.com

Print ISSN: 0331-8443
Electronic ISSN: 2467-8821
http://dx.doi.org/10.4314/njt.v41i1.19

Dynamic Analysis and Computer Simulation of Interior Permanent Magnet Synchronous Motor with Intermittent Loading

C. S. Ezeonye[1,*], I. E. Nkan[2], E. E. Okpo[3], O. I. Okoro[4]

[1,4] *Department of Electrical/Electronic Engineering, Michael Okpara University of Agriculture, Umudike, Abia State, NIGERIA*
[2,3] *Department of Electrical/Electronic Engineering, Akwa Ibom State University, Mpat-Enin, Akwa Ibom State, NIGERIA*

Abstract
This paper presents the dynamic analysis and computer simulation of interior permanent magnet synchronous motor (IPMSM) with intermittent loading. This objective was realized with the aid of MATLAB m.file function program, which is based on an explicit Runge-Kutta fourth order numerical method to solve a set of first order differential system of equations describing electrical and mechanical models of IPMSM. The IPMSM used in this research is of specifications 3-phase, 2 KW, 50 Hz, 4 poles, 240 V. The IPMSM differential equations are expressed in rotor reference frame with q- and d-axes stator currents, mechanical rotor speed, and rotor angular position as state variables. The analysis and simulation of the motor is initially done with no-load and with the parameters as given in Table 1. Subsequently, the motor was loaded and parameter variations were carried out. The result of a typical responses of the motor were obtained which showed that IPMSM has more ripples, overshoot, slower response but can carry load of up to 90 Nm. The effect of higher stator resistance shows that it minimizes the magnitude of ripple of the output characteristics (torque and power) but takes more time to attain the same steady state value. In the same vein, variation of moment of inertia has little or no effect on the output characteristics of the motor. The findings obtained in this research work as compared to other literatures showed that with the parameters recommended, an improved design and operation of IPMSM will be obtained for best performance and without unsynchronous operation due to overloading.

Keywords: Intermittent loading, Interior permanent magnet (IPM), Interior permanent magnet synchronous motor (IPMSM), Neodymium iron-boron (NdFeB), Permanent magnet (PM).

1.0 INTRODUCTION

The permanent magnet materials and the techniques used in driving an electric machine in many industrial applications are replacing induction motors because of interior permanent magnet synchronous motor (IPMSM) advantages in efficiency and size [1]. Simulation of IPMSM is an approach that requires setting up a model of a real situation and carrying out experiments on the model [2]. IPMSM is a type of sinusoidal current synchronous motor that employs permanent magnets to generate magnetic field in the air gap rather than employing electromagnets. They have no windings in the rotor instead they have rotating permanent magnets crafted from neodymium iron-boron (NdFeB), alnico or samarium cobalt that retain their magnetic property. The development in high energy permanent magnets like neodymium iron-boron IPMSM is becoming more popular in high performance and adjustable speed drive applications because it has high air gap flux density of 0.8-1.0 Tesla which can be produced with relatively small magnet volume, high peak torque capability and their linear relationship between torque and stator current.

Some potential limitations of NdFeB material in comparison with other high energy magnets are its relatively low temperature limit and vulnerability to corrosion. These motors have notable features, attracting the concern of researchers and industry for benefit in many industrial applications. These features are high temperature ability, decreasing the risk of demagnetization of permanent magnets, under-excited operation for most load situations, field weakening ability with high inductance, increase in the resistance against corrosion and mechanical impacts, and [3–6]. IPMSM offers the advantages of higher air-gap torque and electromechanical output power per unit volume as compared to electromagnetic excitation, absence of external source of magnetizing current for

*Corresponding author **(Tel:** +234 (0) 8067943870**)**
Email addresses: *ezeonyechinonso@yahoo.com* (C. S. Ezeonye), *imoenkan@yahoo.com* (I. E. Nkan), *okpoekom@yahoo.com* (E. E. Okpo), *oiokoro@yahoo.co.uk* (O. I. Okoro)

excitation, and a negligible rotor loss which means that the loss in the form of heat is avoided which improves the performance operation of the motor. It also offers advantages over other conventional DC motor drives due to the absence of mechanical commutators, less audible noise, higher speed, high power density and smaller size. As compared to induction motors, IPMSMs are preferred because of their superior efficiency, high power density, high torque-to-inertia ratio, high power factor, better heat transfer, absence of rotor slip power loss and the natural ability to supply reactive current and this is the main reason that IPMSM replace the induction motor drives in industry which make them a suitable choice for variable-speed direct-drive applications [7, 8].

The Figure 1 configuration shows that interior permanent magnet rotor construction is mechanically robust and is suitable for higher speeds operations. The IPM rotor has no winding and permanent magnet is replaced by it thereby allowing higher air gaps between the magnets to form flux barriers. They are made to prevent flux passing between adjacent PMs through higher rotor surface. Without these flux barriers, the flux will pass from magnet to the adjacent one through rotor and bypass the stator. Therefore, the mutual flux will be decreased. These barriers reduce rotor weight and thereby rotor inertia constant. Each permanent magnet is mounted inside the rotor and they are protected against armature field. There is variation of inductance for this rotor type configuration due to the permanent magnet part is similar to air in the calculation of magnetic circuit. These motors are taken to have saliency with *q*-axis inductance greater than the *d*-axis inductance ($L_q > L_d$) [9–13]

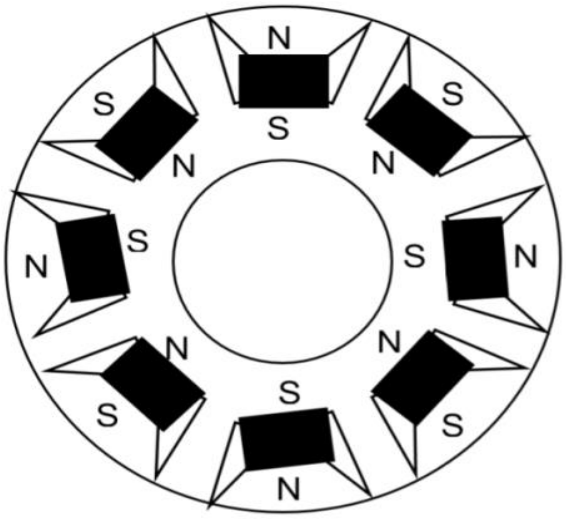

Figure 1: Interior permanent magnet.

Modeling of IPMSM drive system using transient simulation medium was carried out in [6]. In their transient analysis of speed, the effect of intermittent loading was not taken into consideration as it directly affects the transient ripples of the motor speed. Design and analysis of PMSM used in industrial robot was presented in [7]. Their conclusion follows that the design result of PMSM is suitable for industrial robot. Hence the periodic loading of the motor which affects the speed and torque of the motor were not considered. Efficiency assessment of IPMSM using the technique of synthetic loading with MATLAB medium was presented in [12]. Their findingss reveal that the technique of synthetic loading can evaluate the efficiency of IPM synchronous machines. However, they did not show how intermittent loading affects the performance of IPMSM. Design and analysis of IPMSM for Hybrid electric vehicles (HEV) was described in [13] using Finite Element Analysis (FEA). In [14], synthetic loading technique used for to the PM synchronous machine was analyzed and presented using MATLAB and their findings showed that the technique can evaluate the losses associated with PM synchronous machine. Mathematical modeling and simulation of PMSM using Simulink was presented in [15]. Their findings showed that the performance characteristics of PMSM speed remained constant even with variation of load torque. However, they did not substantiate the maximum load that can be applied to the motor. A Study of IPMSMs for HEV traction drive application was proposed in [16] using a novel structure of interior PMSMs for traction applications and this was simulated using a 3-dimensional finite element method model. Transient and steady state operations of two Line Start PMSM with different types of rotor was investigated in [17] using embedded MATLAB function tool. Their findings showed that the loading ability of the SPM rotor is better as compared to IPM rotor on asynchronous rotation as it has slighter torque ripples and IPM motor attains higher responses in terms of speed than SPM motor. However, they did not show the maximum load each motor can sustain without unsynchronous operation. Core loss and saliency effect of IPMSM and SPMSM were analyzed in [18] in which speed was considered as one of the motor characteristics, but they did not show how the effect of intermittent loading affects the motor speed during operation.

From the reviewed literatures, it is seen that the effect of intermittent loading to the output characteristics as applied to the IPMSM was lacking in their analysis as well as the effect of variation in stator resistance and inertia constant. As a result, this paper seeks to analyze using MATLAB the effects of intermittent loading on IPMSM to determine the maximum load the motor can sustain without loss of synchronism and the effect of variation of stator resistance and inertia constant to

determine their sensitivity to the operation of the motor and that required for motor best operating performance.

2.0 METHODOLOGY

The model equations of IPMSM are obtained using a two-phase motor in direct and quadrature axes. The *d*-*q* model has been established on rotor reference frame as depicted in Figure 2. At any time, t, the *d*-axis of the rotating rotor makes an angle θr with the phase axis of the fixed stator and the MMF of the rotating stator makes an angle α with the *d*-axis of the rotor. The MMF of the stator and rotor rotates at the same speed [10, 18].

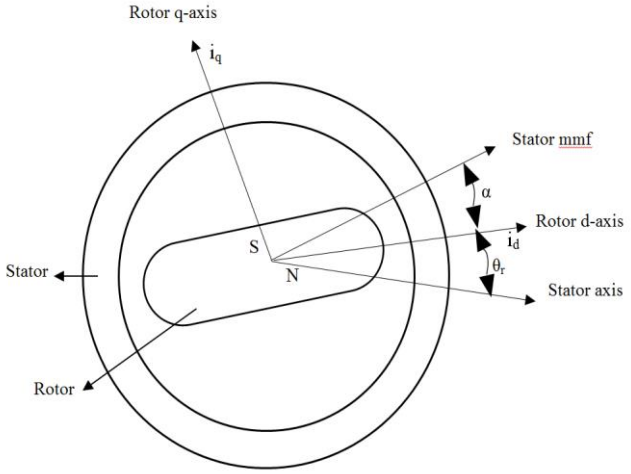

Figure 2: Permanent magnet motor axes.

The assumptions used in developing the models of IPMSM are: Saturation is neglected, the back emf is sinusoidal, and the eddy current and hysteresis losses are ignored.

2.1 Electrical Model of IPMSM

The equivalent circuit of IPMSM is shown in Figure 3, while Equations (1) to (14) are the voltage, current and flux linkage of the motor [19].

The *d*- and *q*-axis voltage equations are given by:

$$V_q = R_s i_q + \rho(\lambda_q) + \omega_r \lambda_d \quad (1)$$

$$V_d = R_s i_d + \rho(\lambda_d) - \omega_r \lambda_q \quad (2)$$

where

ρ: Operator $\frac{d}{dt}$

V_q and V_d: *q*- and *d*-axis voltages

i_q and i_d: *q*- and *d*-axis currents

λ_q and λ_d: *q*- and *d*-axis flux linkages

R_s: Stator resistance

ω_r: Electrical speed of the rotor.

The *q* and *d*-axes flux linkages in the rotor reference frame are

$$\lambda_q = L_q i_q \quad (3)$$

$$\lambda_d = L_d i_d + \lambda_m \quad (4)$$

where

L_q and L_d: *q*- and *d* -axis inductances

λ_m: Rotor flux linkage.

Substituting Equations (3) and (4) in Equations (1) and (2)

$$V_q = R_s i_q + \rho(L_q i_q) + \omega_r (L_d i_d + \lambda_m) \quad (5)$$

$$V_d = R_s i_d + \rho(L_d i_d + \lambda_m) - \omega_r (L_q i_q) \quad (6)$$

Where $\rho(\lambda_m) = 0$

Resolving further,

$$V_q = (R_s + \rho L_q) i_q + \omega_r L_d i_d + \omega_r \lambda_m \quad (7)$$

$$V_d = -\omega_r L_q i_q + (R_s + \rho L_d) i_d \quad (8)$$

Putting Equations (7) and (8) in matrix form,

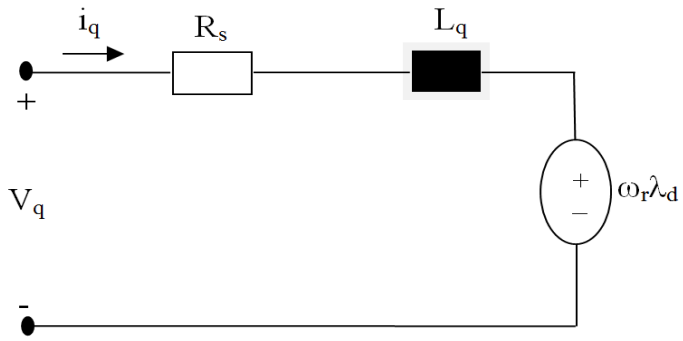

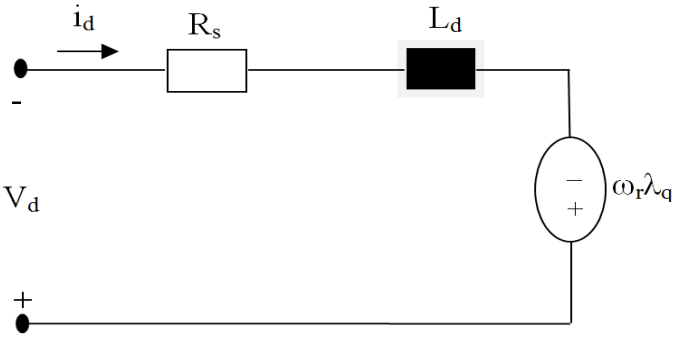

Figure 3: Equivalent circuit of IPMSM.

$$\begin{bmatrix} V_q \\ V_d \end{bmatrix} = \begin{bmatrix} (R_s + \rho L_q) & \omega_r L_d \\ -\omega_r L_q & (R_s + \rho L_d) \end{bmatrix} \begin{bmatrix} i_q \\ i_d \end{bmatrix} + \begin{bmatrix} \omega_r \lambda_m \\ 0 \end{bmatrix} \quad (9)$$

$$\lambda_m = \lambda_{af} = L_m i_{fr} \quad (10)$$

Solving Equations (7) and (8) further gives the following:

$$\frac{di_q}{dt} = -\frac{R_s}{L_q} i_q - \frac{\omega_r L_d}{L_q} i_d + \frac{V_q}{L_q} - \frac{\omega_r \lambda_m}{L_q} \quad (11)$$

$$\frac{di_d}{dt} = \frac{\omega_r L_q}{L_d} i_q - \frac{R_s}{L_d} i_d + \frac{V_d}{L_d} \quad (12)$$

When resistance due to stator core is considered, the axis currents as well as state variable equations becomes

$$\frac{di_q}{dt} = \frac{-R_s R_c}{L_q(R_s + R_c)} i_q - \frac{\omega_r L_d}{L_q} i_d + \frac{V_q R_c}{L_q(R_s + R_c)} - \frac{\omega_r \lambda_m}{L_q} \quad (13)$$

$$\frac{di_d}{dt} = \frac{\omega_r L_q}{L_d} i_q - \frac{R_s R_c}{L_d(R_s + R_c)} i_d + \frac{V_d R_c}{L_d(R_s + R_c)} \quad (14)$$

Where R_c is stator core resistance

2.2 Mechanical Model of IPMSM

Equations (15) to (21) represent the mechanical equations of the motor, which include torque, power, and rotor speed.

The general mechanical equation for the motor is given as:

$$T_e = T_l + T_d + B\omega_{rm} + J\rho\omega_{rm} \quad (15)$$

where
ω_{rm}: Mechanical speed of the rotor
B: Viscous frictions coefficient
J: Inertia of the shaft and the load system
T_d: Dry friction torque
T_l: Load torque
T_e: Electromagnetic torque
From Equation (15), we have

$$\frac{d\omega_{rm}}{dt} = \frac{-B}{J}\omega_{rm} + \frac{1}{J}(T_e - T_l) \quad (16)$$

Also,

$$\frac{d\theta_r}{dt} = \omega_r \quad (17)$$

Where θ_r is the electrical rotor angular position
Electromagnetic torque of the motor in terms of *q*- and *d*-axis flux linkages, rotor flux linkage, and *q*- and *d*-axis inductances as stated in [20, 21] is given as:

$$T_e = \frac{3}{2}\left(\frac{P}{2}\right)(\lambda_d i_q - \lambda_q i_d) \quad (18)$$

Substituting the *q*- and *d*-axes flux linkages of Equations (3) and (4) in Equation (18) gives

$$T_e = \frac{3}{2}\left(\frac{P}{2}\right)(\lambda_m i_q + (L_d - L_q) i_q i_d) \quad (19)$$

Electromechanical power of the motor is given as

$$P_{em} = \omega_{rm} T_e = \frac{3}{2}\omega_r(\lambda_d i_q - \lambda_q i_d) \quad (20)$$

The mechanical speed N (that is synchronous speed) in terms of revolutions per minute (rpm) can be stated as

$$N = \frac{60}{2\pi} \times \omega_{rm} = \frac{30}{\pi} \times \omega_{rm} \quad (21)$$

Combining Equations (11), (12), (13), (14), (16) and (17) in state variable form where i_q, i_d, ω_{rm}, and θ_r form the state vectors by which other motor characteristics can be determined. Equation (22) represents the state vector of the IPMSM when stator core resistance, R_c is not considered, while Equation (23) represents the state vector of the IPMSM when stator core resistance, R_c is considered.

$$\frac{d}{dt}\begin{bmatrix} i_q \\ i_d \\ \omega_{rm} \\ \theta_r \end{bmatrix} = \begin{bmatrix} \frac{-R_s}{L_q} & \frac{-\omega_r L_d}{L_q} & 0 & 0 \\ \frac{\omega_r L_q}{L_d} & \frac{-R_s}{L_d} & 0 & 0 \\ 0 & 0 & \frac{-B}{J} & 0 \\ 0 & 0 & 0 & 0 \end{bmatrix} \begin{bmatrix} i_q \\ i_d \\ \omega_{rm} \\ \theta_r \end{bmatrix} + \begin{bmatrix} \frac{1}{L_q}(V_q - \omega_r \lambda_m) \\ \frac{V_d}{L_q} \\ \frac{1}{J}(T_e - T_l) \\ \omega_r \end{bmatrix} \quad (22)$$

$$\frac{d}{dt}\begin{bmatrix} i_q \\ i_d \\ \omega_{rm} \\ \theta_r \end{bmatrix} = \begin{bmatrix} \frac{-R_s R_c}{L_q(R_s+R_c)} & \frac{-\omega_r L_d}{L_q} & 0 & 0 \\ \frac{\omega_r L_q}{L_d} & \frac{-R_s R_c}{L_d(R_s+R_c)} & 0 & 0 \\ 0 & 0 & \frac{-B}{J} & 0 \\ 0 & 0 & 0 & 0 \end{bmatrix} \begin{bmatrix} i_q \\ i_d \\ \omega_{rm} \\ \theta_r \end{bmatrix} + \begin{bmatrix} \frac{1}{L_q}\left(\frac{V_q R_c}{R_s+R_c} - \omega_r \lambda_m\right) \\ \frac{V_d R_c}{L_d(R_s+R_c)} \\ \frac{1}{J}(T_e - T_l) \\ \omega_r \end{bmatrix} \quad (23)$$

2.3 Dynamic d- and q-Axis Modeling and Park Transformation

The dynamic *dq* modeling is used for the analysis of IPMSM during transient and steady state. It is done by transforming the three phase currents and voltages to *dq* variables by using Park's transformation [10, 22].

The reference frame voltages of IPMSM under balance condition can be estimated as:

$$V_a = \sqrt{2}V\cos\omega_b t \quad (24)$$

$$V_b = \sqrt{2}V\cos(\omega_b t - \frac{2\pi}{3}) \quad (25)$$

$$V_c = \sqrt{2}V\cos(\omega_b t + \frac{2\pi}{3}) \quad (26)$$

where

$\omega_b = 2\pi f$ is the rated source frequency in rad/s

V_a, V_b, and V_c: Stator phase a, b, c voltages

V: Line voltage

The three phase stator voltages are related to *q*- and *d*-axis reference frame as follows:

$$\begin{bmatrix} V_q \\ V_d \end{bmatrix} = \frac{2}{3}\begin{bmatrix} \cos\theta & \cos(\theta-120) & \cos(\theta+120) \\ \sin\theta & \sin(\theta-120) & \sin(\theta+120) \end{bmatrix}\begin{bmatrix} V_a \\ V_b \\ V_c \end{bmatrix} \quad (27)$$

$$\begin{bmatrix} V_a \\ V_b \\ V_c \end{bmatrix} = \begin{bmatrix} \cos\theta & \sin\theta \\ \cos(\theta-120) & \sin(\theta-120) \\ \cos(\theta+120) & \sin(\theta+120) \end{bmatrix}\begin{bmatrix} V_q \\ V_d \end{bmatrix} \quad (28)$$

Likewise, the three phase currents can be calculated in the same way as:

$$\begin{bmatrix} i_q \\ i_d \end{bmatrix} = \frac{2}{3}\begin{bmatrix} \cos\theta & \cos(\theta-120) & \cos(\theta+120) \\ \sin\theta & \sin(\theta-120) & \sin(\theta+120) \end{bmatrix}\begin{bmatrix} i_a \\ i_b \\ i_c \end{bmatrix} \quad (29)$$

$$\begin{bmatrix} i_a \\ i_b \\ i_c \end{bmatrix} = \begin{bmatrix} \cos\theta & \sin\theta \\ \cos(\theta-120) & \sin(\theta-120) \\ \cos(\theta+120) & \sin(\theta+120) \end{bmatrix}\begin{bmatrix} i_q \\ i_d \end{bmatrix} \quad (30)$$

Where i_a, i_b, and i_c are stator phase a, b, c currents while θ is the phase angle.

3.0 RESULTS AND DISCUSSION

This section introduces the simulation results of performances of the IPMSM by using MATLAB m-file to observe the various characteristics with time on intermittent loading. The analysis is validated by using the machine data as shown in Table 1. The machines' parameters are obtained by carrying out the FEA on the test motors using Maxwell2D/RMxprt [23].

Table 1: Motor parameters for IPMSM

Motor Parameter	Value
Rated power, P	2 kW
Rated voltage, V	240 V
Rated speed, ω	1500 rpm
q-axis inductance, L_q	11.8 mH
d-axis inductance, L_d	4.6 mH
Rotor flux linkage, λ_{af}	1.14 mWb
Number of poles, P	4
Stator resistance, R_s	0.86 Ω
Stator core resistance, R_c	18 Ω
Inertia coefficient, J	0.00021 kg/m^2
Load torque, T_l	0 Nm
Dry friction, T_d	0 Nm
Frequency, f	50 Hz
Viscous friction coefficient, B	0.015 Nms

Figure 4 shows the three-phase voltage which is fed to the stator of the IPMSM to set up the stator currents i_a, i_b, and i_c. The magnitude of the three phase stator voltage is 339 volts which is the product of V_{rms} and square root of 2. Figure 5 shows the stator currents at a phase difference of 120 degrees each. The current is non-sinusoidal at the starting and becomes sinusoidal when the motor reaches its steady state of 80 amperes at 0.05 seconds.

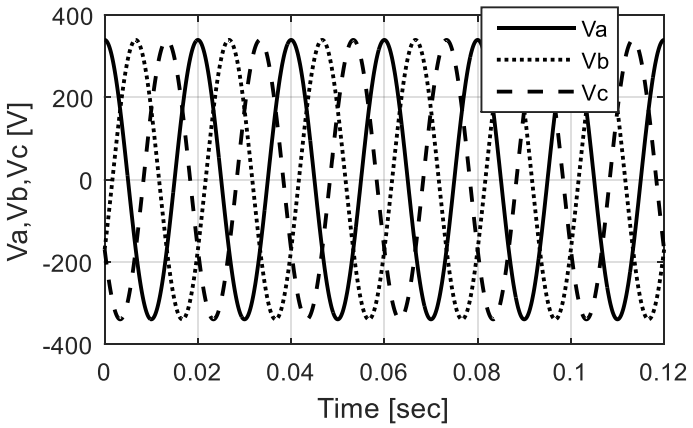

Figure 4: Graph of stator voltage against time.

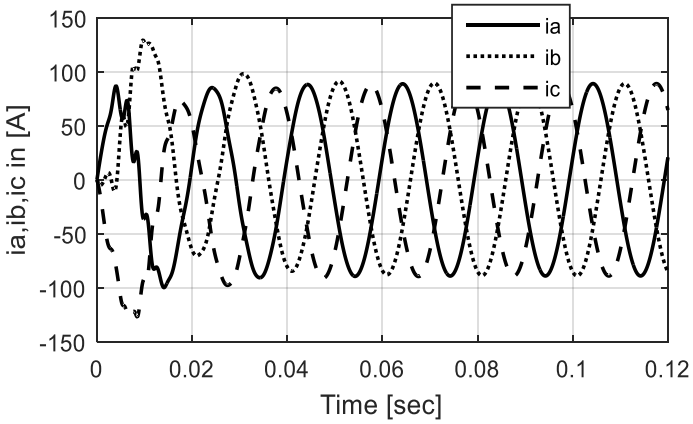

Figure 5: Graph of stator current against time.

Figure 6 shows the output power of the motor which attained their steady state value of 0.5 kw at 0.05 seconds and the magnitude of the ripple during transient is 11 kw and Figure 7 shows mechanical rotor speed which attained steady state value of 157 rad/s and peak magnitude of ripples which is due to vibrations that occur during starting stood at 240 rad/s.

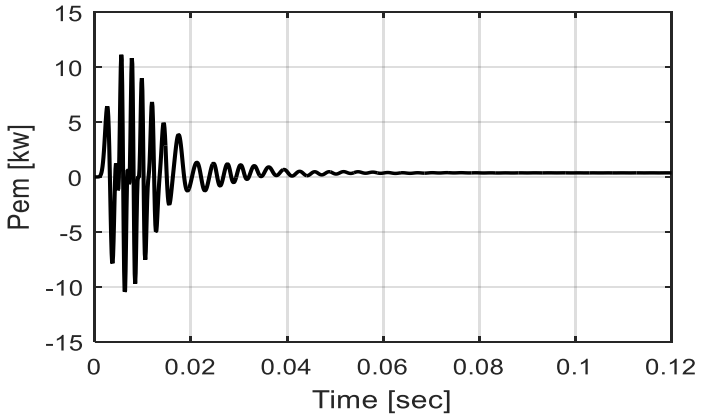

Figure 6: Graph of electromechanical power against time.

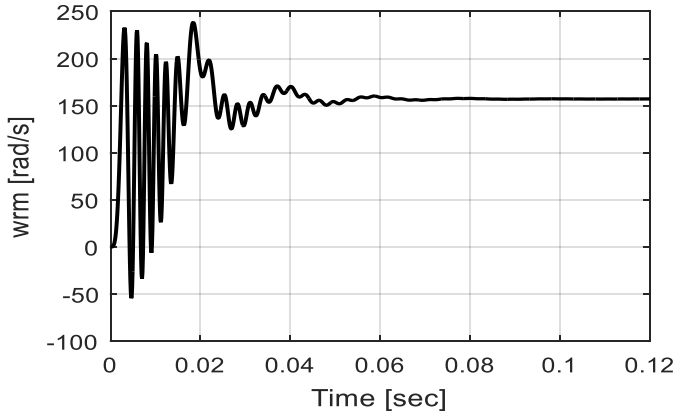

Figure 7: Graph of mechanical rotor speed against time.

In Figure 8, it is seen that when R_c equals zero, it increased the steady state magnitude of phase currents to 90 A, while when R_c of 18 Ohms is introduced, the steady state values of stator currents dropped to 50 A.

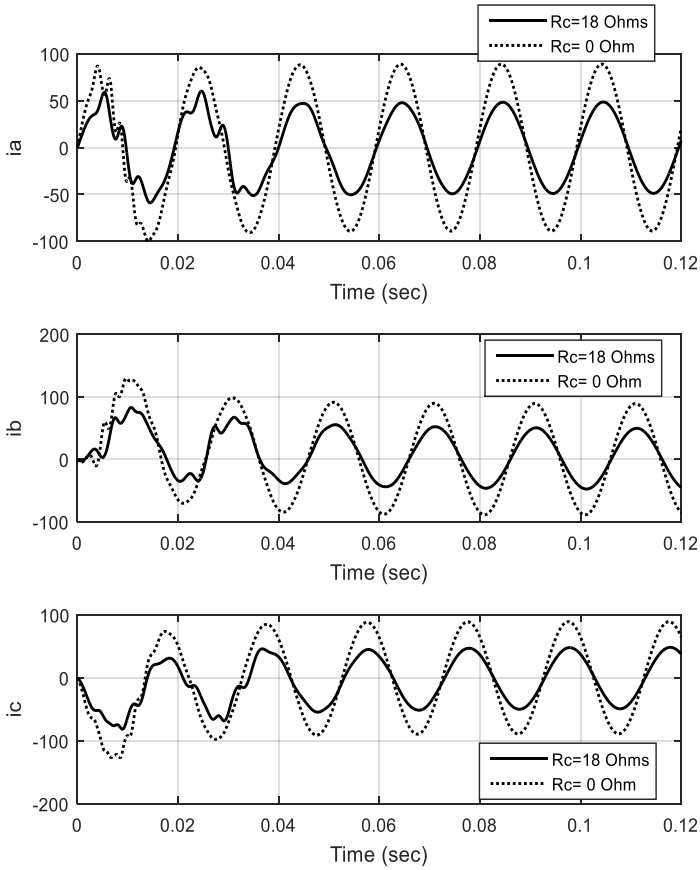

Figure 8: Graph of phase currents with Rc.

From Figures 9, and 10, it is seen that as resistance due to stator core is increased to 18 Ohms, more ripples are introduced in the output power and electromagnetic torque responses and it took more time to attain the steady state values of 0.5 kw and 3 Nm respectively.

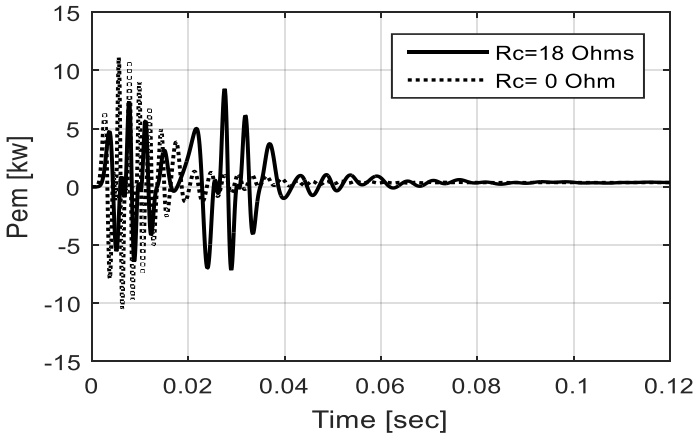

Figure 9: Graph of electromechanical power with Rc.

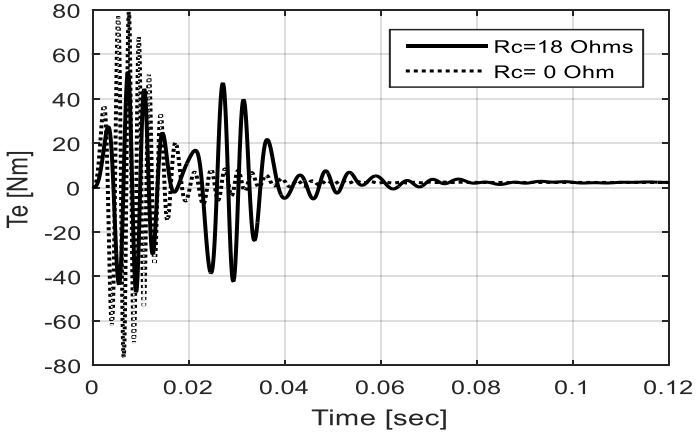

Figure 10: Graph of electromagnetic torque with Rc.

From Figure 11, it is seen that as stator resistance, R_s is decreased from 0.86 ohm to 0.43 ohm, the magnitude of the torque ripple increases from 75 Nm to 110 Nm and it takes more time to attain its steady state, but the steady state of the electromagnetic torque remains the same at 3 Nm.

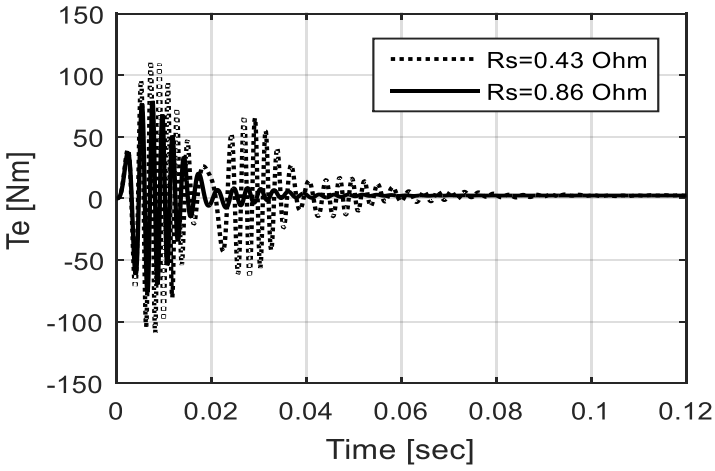

Figure 11: Graph of electromagnetic torque with variable Rs.

In Figure 12, decrease in inertia coefficient from 2.1e-4 kg/m^2 to 1.05e-4 kg/m^2 gives less distortion during transient and takes less time to attain its steady state as compared to higher values. Both variations maintained the same values of steady state.

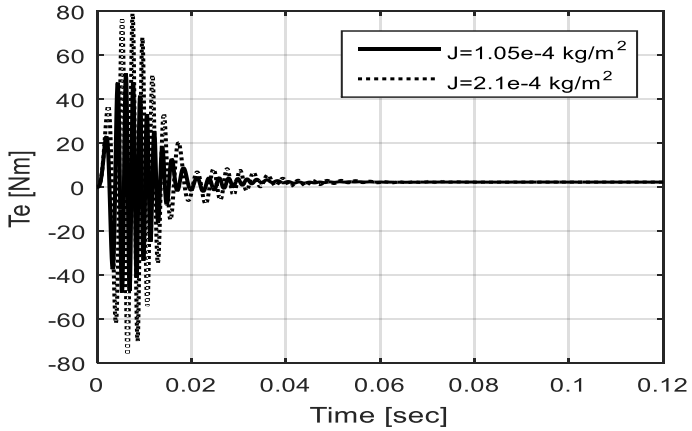

Figure 12: Graph of electromagnetic torque with variable J.

From Figures 13 and 14, as load increases, the steady state value of electromagnetic torque increases and ripple magnitude decreases. In Figure 13, when the load is disconnected from 90 Nm to 0 Nm after 0.275 second, this led to the increase in ripple magnitude to 75 Nm while in Figure 14, the load is disconnected in step from 90 Nm to 60 Nm to 30 Nm to 0 Nm and in this way the peak magnitude of the ripple is reduced.

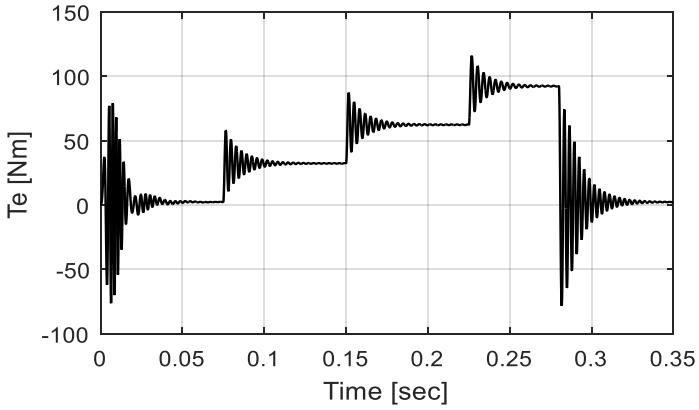

Figure 13: Electromagnetic torque response on loading.

It is seen from Figures 15 and 16 that the effect of intermittent load does not affect the steady state value of the speed rather it affects the ripple. In Figure 15, the load is disconnected to 0 Nm after 0.275 second and this led to the increase in ripple magnitude to 790 rad/sec while in Figure 16, the load is disconnected in steps and in this way the peak magnitude of the ripple reduced to 485 rad/sec. The steady state value of speed remains constant at 314 rad/s irrespective of load variation.

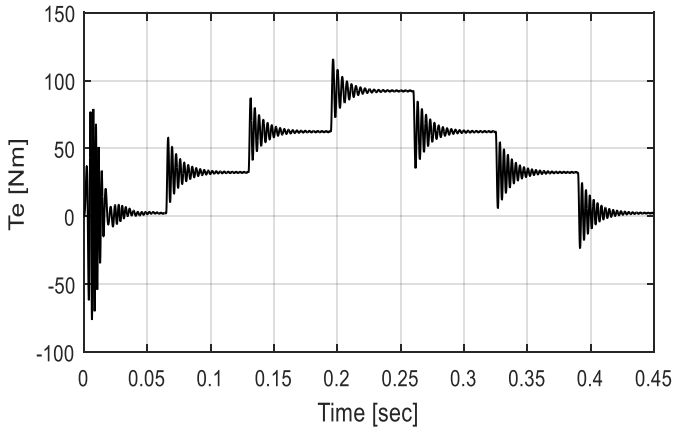

Figure 14: Electromagnetic torque response on loading.

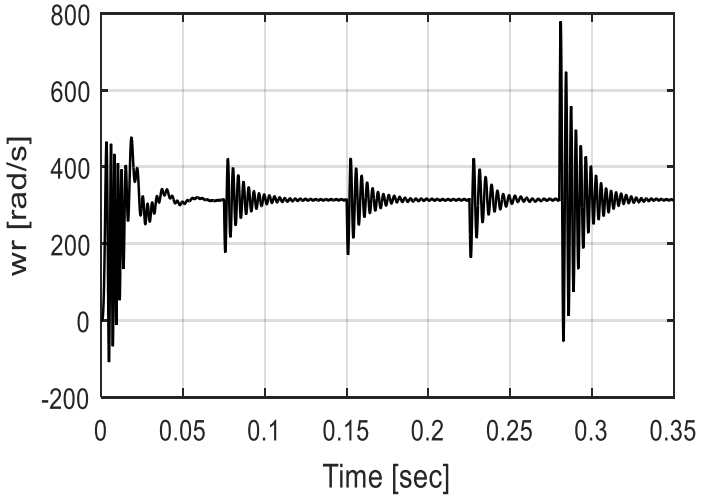

Figure 15: Electrical rotor speed response on loading.

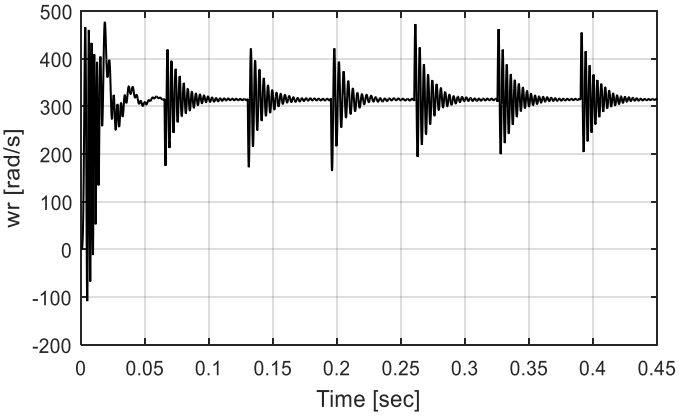

Figure 16: Electrical rotor speed response on loading.

At 101 Nm as it is seen on Figures 17 and 18, the response of the motor parameters (electromagnetic torque and mechanical output power) became unsteady and hence unsynchronous operation. This implies that motor with parameters in Table 1 cannot be loaded beyond 100 Nm.

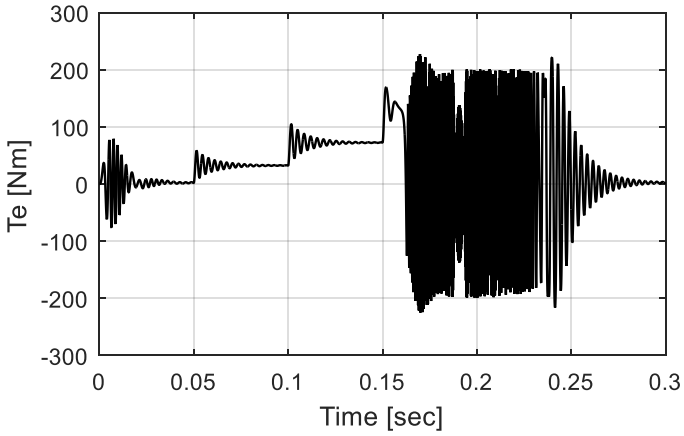

Figure 17: Electromagnetic torque response on loading beyond 100 Nm.

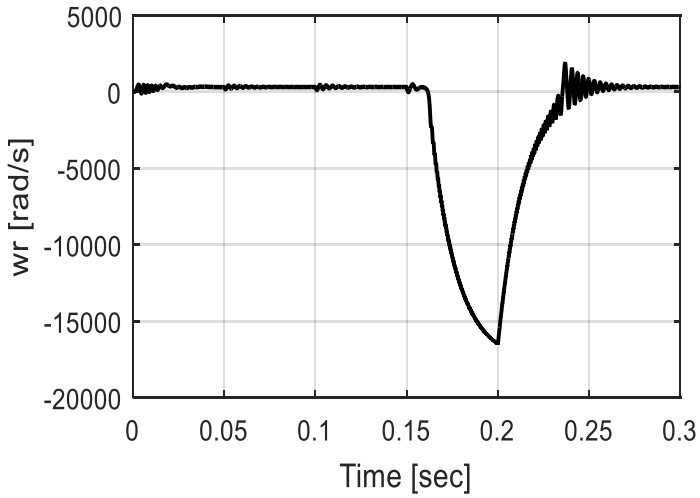

Figure 18: Electrical rotor speed on loading beyond 100 Nm.

4.0 CONCLUSION

In this research paper, dynamic analysis and computer simulation-based behaviour of IPMSM with intermittent loading is implemented using MATLAB m-file. The analysis and simulation results and findings show that when the resistance due to stator core is increased, the steady state magnitude of phase currents decreases, and it took more time to attain the steady states values of electromechanical output power and electromagnetic torque. It is also seen from torque response that when stator resistance is decreased, the peak magnitude of ripples increases while when inertia constant is decreased, it has little or no effect on the steady state as well as peak magnitude of ripples. This implies that in the design of IPMSM, the stator resistance should not be below that given in Table 1 and inertia constant should be equal or 50% less to the one in Table 1. It is also seen that IPMSM shows more ripples, overshoot, slower response and can

carry load of up to 90 Nm but cannot be loaded beyond 100 Nm otherwise the motor will go out of synchronism.

REFERENCES

[1] Seong, T. L. "Development and Analysis of Interior Permanent Magnet Synchronous Motor with Field Excitation Structure", Ph. D. Dissertation, University of Tennessee, Knoxville, USA, 2009.

[2] Okoro, O. I. "Introduction to Matlab/Simulink for Engineers and Scientists", 2nd edition. John Jacob's Classic Publishers Ltd, Enugu, 2008.

[3] Qinghua, L. "Analysis, Design and Control of Permanent Magnet Synchronous Motors for Wide-Speed Operations", Ph.D Thesis, National University of Singapore, 2005.

[4] Remitha, K. M. and Anna, M. "Matlab/Simulink Model of Field Oriented Control of Permanent Magnet Synchronous Motor Drive using Space Vectors", *International Journal of Advances in Engineering & Technology*, 6(3), 2013, pp. 1355-1364.

[5] Mishra, A., Agarwal, P. and Srivastava, S. P. "A Comprehensive Analysis and Implementation of Vector Control of Permanent Magnet Synchronous Motor", *International Journal of Power and Energy Conversion*, 5(1), 2014, pp. 1-23.

[6] Parvathi, M. S. and Nisha, G. K. "Modeling of Interior Permanent Magnet Synchronous Motor using Transient Simulation Techniques", *International Journal of Innovative Science, Engineering & Technology*, 3(7), 2016, pp. 409-413.

[7] Aye, A. T. and Aung, Z. Y. "Design and Analysis of Permanent Magnet Synchronous Motor (PMSM) used in Industrial Robot", *Fourth National Conference on Science and Engineering, Mandalay, Myanmar*, June 1-2, 2011, pp. 1-4.

[8] Ritu, T., Sudhir, Y. K. and Rajpurohit, B. S. "Dynamic Modeling of Surface Mounted Permanent Synchronous Motor for Servo Motor Application", *International Journal of Scientific Research Engineering & Technology (IJSRET)*, 6(8), 2017, pp. 797-802.

[9] Bose, B. K. "Modern Power Electronics and AC Drives", Prentice Hall PTR, New Jersey, 2002.

[10] Arroyo, E. L. C. "Modeling and Simulation of Permanent Magnet Synchronous Motor Drive System", M. Sc. Thesis, University of Puerto Rico, Mayaguez, 2006.

[11] Shady, M. S. A. "Direct Torque Control of Permanent Magnet Synchronous Motors (DTC PMSM)", M. Sc. Thesis, Cairo University, Giza, 2016.

[12] Abbas, A. Y. M. and Fletcher, J. E. "Efficiency Evaluation of Interior Permanent Magnet Synchronous Machines using the Synthetic Loading Technique", *International Symposium on Power Electronics, Electrical Drives, Automation and Motion*, Pisa, Italy, June 14-16, 2010, pp. 7-12.

[13] Venkata, K. A. K. and Latha, K. "Design and Analysis of Interior Permanent Magnet Synchronous Motor (IPMSM) for Hybrid Electric Vehicles (HEV)", *Institute of Electrical and Electronics Engineers Industry Applications Society Annual Meeting*, Houston, USA, October 3-7, 2010, pp. 1-4.

[14] Abbas, A. Y. M. and Fletcher, J. E. "The Synthetic Loading Technique Applied to the PM Synchronous Machine", *Institute of Electrical and Electronics Engineers Transactions on Energy Conversion*, 26(1), 2011, pp. 83-92.

[15] Siva, G. R. V., Sneha, V. and Sravani, M. "Mathematical Modeling and Simulation of Permanent Magnet Synchronous Motor", *International Journal of Advanced Research in Electrical Electronics and Instrumentation Engineering*, 2(8), 2013, pp. 3720-3726.

[16] Javad, S., Abolfazl, V., Abdolhossein, E. and Mohammadhossein, B. B. "Study on Interior Permanent Magnet Synchronous Motors for Hybrid Electric Vehicle Traction Drive Application Considering Permanent Magnet Type and Temperature", *Turkish Journal of Electrical Engineering & Computer Sciences*, 22, 2014, pp. 1517-1527.

[17] Asogwa, J. C. and Obe, E. S. "Investigation of the Transient and Steady State Operations of Two Line Start Permanent Magnet Motors (LSPMMS) with Different Rotor Configurations", *Nigerian Journal of Technology (NIJOTECH)*, 38(1), 2019, pp. 185-192.

[18] Ezeonye, C. S., Okpo, E. E., Nkan, I. E. and Okoro, O. I. "Effect of Saliency and Core Losses on the Dynamic Behavior of Permanent Magnet Synchronous Motor", *Bayero Journal of Engineering and Technology (BJET)*, 15(3), 2020, pp. 124-133.

[19] Kim, S. A., Song, J. H., Han, S. W. and Cho, Y. H. "An Improved Modeling of Permanent Magnet Synchronous Machine with Torque Ripple Characteristics", *Journal of Clean Energy Technologies*, 6(2), 2018, pp.117-120.

[20] El Shewy, H. M., Abd Al Kader, F. E., El Kholy, M. M. and El Shahat, A. "Dynamic Modeling of Permanent Magnet Synchronous Motor Using MATLAB – Simulink", *6th International*

Conference on Electrical Engineering (ICEENG), Cairo, Egypt, May 27-29, 2008, pp.1-16.

[21] El Shahat, A. and El Shewy, H. M. "Permanent Magnet Synchronous Motor Dynamic Modeling with Genetic Algorithm Performance Improvement", *International Journal of Engineering, Science and Technology*, 2(2), 2010, pp.93-106.

[22] Krause, P., Wasynczuk, O., Sudhoff, S. and Pekarek, S. "Analysis of Electric Machinery and Drive Systems", 3rd edition. John Wiley & Sons, Inc., New Jersey, 2013.

[23] Maxwell 2D/RMxPrt FEA-Simulation Program. "Ansoft Corporation", Munich, 2010.